Lamin A upregulation reorganizes the genome during rod photoreceptor degeneration

Ivana Naď
Ottawa Hospital Research Institute

José Fernandes
Ottawa Hospital Research Institute   https://orcid.org/0000-0003-2995-5452

Khatereh Shir-Mohammadi
Ottawa Hospital Research Institute

Pierre Mattar (✉ pmattar@ohri.ca)
Ottawa Hospital Research Institute   https://orcid.org/0000-0002-5708-6218

Article

Keywords:

Additional Declarations: (Not answered)

1   **Lamin A upregulation reorganizes the genome during rod photoreceptor degeneration**

2

3   Ivana Nađ[1,2], José Alex Lourenço Fernandes[1,2], Khatereh Shir-Mohammadi[1,2], Pierre Mattar[1,2,*]

4

5

6   [1]Ottawa Hospital Research Institute (OHRI), Ottawa, ON, K1H 8L6

7   [2]Department of Cellular and Molecular Medicine, University of Ottawa, Ottawa, ON, K1H 8M5

8

9   * Correspondence to: pmattar@ohri.ca

10

11   Main text: 3261 words

12   **Running Title:**

13   Lamin A upregulation reorganizes the rod genome

14 **Abstract:**

15

16 Neurodegenerative diseases are accompanied by dynamic changes in gene expression,

17 including the upregulation of hallmark stress-responsive genes. While the transcriptional

18 pathways that impart adaptive and maladaptive gene expression signatures have been the

19 focus of intense study, the role of higher order nuclear organization in this process is less clear.

20 Here, we examine the role of the nuclear lamina in genome organization during the

21 degeneration of rod photoreceptors. Two proteins had previously been shown to be necessary

22 and sufficient to tether heterochromatin at the nuclear envelope. The lamin B receptor (Lbr) is

23 expressed during development, but downregulates upon rod differentiation. A second tether is

24 the intermediate filament lamin A (LA), which is not normally expressed in murine rods. Here,

25 we show that in the *rd1* model of retinitis pigmentosa, LA ectopically upregulates in rod

26 photoreceptors at the onset of degeneration. LA upregulation correlated with increased

27 heterochromatin tethering at the nuclear periphery in *rd1* rods, suggesting that LA reorganizes

28 the nucleus. To determine how heterochromatin tethering affects the genome, we used in vivo

29 electroporation to misexpress LA or Lbr in mature rods in the absence of degeneration,

30 resulting in the restoration of conventional nuclear architecture. Using scRNA-seq, we show

31 that reorganizing the nucleus via LA/Lbr misexpression has relatively minor effects on rod gene

32 expression. Next, using ATAC-seq, we show that LA and Lbr both lead to marked increases in

33 genome accessibility. Novel ATAC-seq peaks tended to be associated with stress-responsive

34 genes. Together, our data reveal that heterochromatin tethers have a global effect on genome

35   accessibility, and suggest that heterochromatin tethering primes the photoreceptor genome to

36   respond to stress.

Introduction

Photoreceptor cells are highly susceptible to degeneration – perhaps due to their very high metabolic demands[1]. Cone photoreceptors are responsible for high-acuity color vision, whereas rod photoreceptors mediate vision in low-light conditions. Indeed, rods are sensitive enough to respond to individual photons[2]. To achieve this feat, rods must maintain high-level expression of at least 50 genes that can lead to degeneration when misregulated[3, 4]. Genome regulation is thus essential for photoreceptor survival.

The importance of genome organization in photoreceptors is further underscored by their specialized nuclear architecture. In mice, rods undergo a process called "chromatin inversion"[5, 6, 7]. Whereas most cells tether heterochromatin in 'lamina-associated domains' at the nuclear periphery, rod photoreceptors localize heterochromatin centrally[5, 6, 7, 8]. Throughout mammalian evolution, chromatin inversion is correlated with nocturnal lifestyle, as the inverted configuration decreases light scattering and enhances contrast sensitivity[7, 9]. At the molecular level, two proteins have been shown to be sufficient for heterochromatin tethering.

1) The lamin B receptor (Lbr) is a multi-pass transmembrane receptor that contains an intra-nuclear tudor domain. Murine rods naturally express Lbr during development, although Lbr levels decline once rods differentiate. However, when Lbr expression in rods was artificially sustained, chromatin inversion was prevented[10].

59   2) The *Lmna* gene encodes two splice variants – lamin A (LA) and lamin C (LC), neither of which

60   is normally expressed in murine rod photoreceptors[10, 11, 12, 13]. These A-type lamins are

61   intermediate filaments that form a meshwork across the surface of the inner nuclear

62   membrane. In *Lmna* knockout mice, heterochromatin tethering was lost in various tissues, but

63   transgenic misexpression of LC in rods had no effect on their inverted organization[10], initially

64   suggesting that A-type lamins were *not* sufficient for heterochromatin tethering. However, we

65   recently showed that LA is sufficient to tether heterochromatin in rods[12], resolving this

66   conundrum.

67

68   Interestingly, mice harboring mutations in a variety of chromatin proteins have been shown to

69   lose their inverted organization[10, 12, 14, 15, 16, 17, 18]. However, A-type lamins have been shown to

70   upregulate in some of these knockouts[10, 12, 15], raising the possibility that heterochromatin

71   tethers might contribute to degeneration-associated nuclear reorganization.

72

73   Here, we show that LA upregulates in the *rd1* mouse – one of the best studied models for

74   retinitis pigmentosa. Rod degeneration in the *rd1* mutant is triggered via toxic accumulation of

75   cyclic guanosine monophosphate - a chromatin-independent process. Using genomic and

76   transcriptomic approaches, we find that heterochromatin tethering may help to reconfigure the

77   genome to respond to stress.

78

79   **Results**

80

81   *Lamin A upregulates during rod photoreceptor degeneration*

82

83   LA is sufficient to reorganize the rod nucleus[12], whereas LC has no effect[10]. We and others

84   reported LA/LC upregulation in mutant rods[10, 12, 15]. However, our previous work did not

85   discriminate between LA and LC. Using an isoform-specific antibody (Fig. S1A), we found that in

86   wild-type mice, LA was extensively expressed within the inner retina (Fig. 1A, B), as reported

87   previously[13]. In photoreceptors, LA immunoreactivity was observed only in cones (Fig. 1A, B,

88   arrowheads), and was absent from rods (Fig. 1A, B). *Lmna* transcription was also little detected

89   in chick, human, or macaque rods as determined via the *Plae* scRNA-seq database[19] (Fig. S1B).

90

91   Previous studies revealed nuclear disorganization and LA/LC upregulation in mice harboring

92   mutations in essential chromatin proteins (eg. Casz1, Atxn7), but whether this was a general

93   feature of degeneration remained unclear. To address this question, we examined *rd1* mice – a

94   well-studied degenerative model in which rods are completely eliminated by the fourth

95   postnatal week. The *rd1* mutation disrupts the *Pde6b* gene, which is linked to retinitis

96   pigmentosa in humans[20]. Examination of P16 *rd1* mice revealed extensive LA expression within

97   the degenerating photoreceptor layer (Fig. 1C). Since cone cell death is more protracted versus

98   rods in the *rd1* model, we co-stained *rd1* retinas with the rod-specific transcription factor Nr2e3

99   (Fig. 1C, D; Supplemental Movie). This confirmed that LA upregulated in *bona fide* rods in the

100   *rd1* retina.

101

102

103   To corroborate these observations, we examined a recently published RNA-seq dataset made

104   from sorted *rd1* rods[21]. In this dataset, *Lmna* was among the most significantly upregulated

105   genes[21]. Moreover, *Lmna* upregulation coincided precisely with the onset of cell death at P10

106   (Fig. 1E). To determine how this upregulation related to the *LA* splice variant, we re-mapped

107   Jiang et al.'s RNA-seq data. Examination of *Lmna* exon usage revealed that alternative splicing

108   generated lesser but nonetheless significant levels of *LA* versus *LC* (Fig 1F, G). Finally, we

109   examined *Lbr* transcripts, but found no difference in wild-type versus *rd1* mice (Fig. 1H). Thus,

110   degenerating rods upregulate LA, raising the possibility that higher order genome organization

111   might be reconfigured in these photoreceptors.

112

113   To test this idea directly, we measured heterochromatin tethering in LA–positive versus –

114   negative rods. We found that the distance between each chromocenter and the margin of the

115   nucleus was significantly reduced in LA+ versus LA–negative rods (Fig. 2A-D). Similarly, the

116   intensity of DNA at the nuclear periphery was elevated in LA+ cells (Fig. 2E), suggesting that LA

117   reorganizes the nucleus during degeneration.

118

119   During cell death, rod nuclei undergo pyknosis – in which chromatin compacts and the nucleus

120   shrinks markedly[22]. However, we found that pyknotic nuclei did not express LA (Fig. 2B;

121   asterisk), suggesting that the upregulation of LA/LC is an early and likely transient event during

122   the degenerative process.

123

124   *Heterochromatin tethering by Lamin A versus Lbr*

125

126   While LA+ rods exhibited increased heterochromatin tethering, *Lbr* is still expressed when LA

127   upregulates (Fig. 1G, H) raising the question of whether LA and Lbr tether heterochromatin

128   differently. To compare LA versus Lbr –dependent heterochromatin tethering, wild-type retinas

129   were electroporated at P0 with control, LA, or Lbr expression constructs cloned into the pCIG2

130   vector, which contains an IRES2-EGFP reporter cassette. Importantly, due to the exclusively

131   embryonic temporal window for cone generation, cone photoreceptors are never transfected[23,]

132   [24, 25]. Transfected rods were examined at P42, when chromatin inversion is complete (Fig. 3A, B;

133   Fig. S2).

134

135   Using morphometric measures for heterochromatin tethering (Fig. 3C, D), we found that both

136   LA and Lbr increased the intensity of DNA at the nuclear periphery equivalently in comparison

137   to control cells (Fig. 3 E-H). However, in Lbr-transfected cells, chromocenters appeared to

138   contact the lamina more directly (Fig. 3G). As a result, the distance between the chromocenter

139   centroid and nuclear lamina was significantly reduced in Lbr-transfected rods versus LA-

140   transfected rods (Fig. 3I).

141

142   *Heterochromatin tethers have subtle effects on gene expression*

143

144   To determine how tethering affects gene expression, we misexpressed LA/Lbr in rods using in

145   vivo electroporation. After 8 weeks, we flow-sorted viable EGFP+ cells. As we were only able to

146   obtain a few thousand cells per transfected retina, we opted to perform scRNA-seq using the

147   10x Genomics Chromium platform. To avoid batch effects, we multiplexed samples using the

148   Multi-seq barcoding approach. After removing low-quality cells and performing additional

149   quality controls (see Methods), we clustered individual cells using Uniform Manifold

150   Approximation and Projection (UMAP; Fig. 4A). To annotate cell types in an unsupervised

151   manner, we used scDeepSort[26] trained on a previously published retinal RNA-seq atlas[27]. As

152   expected, most sorted cells in the dataset were rods, but a few bipolars and Müllers were also

153   annotated (Fig. 4B).

154

155   Focusing solely on annotated rods, Control, LA, and Lbr -transfected cells clustered in an

156   overlapping fashion, suggesting little difference between their overall gene expression patterns

157   (Fig. 4D, E). Similarly, we found that both LA and Lbr misexpression had relatively modest

158   effects on the expression of individual genes (Fig. 4E, F; Table S1). Characteristic photoreceptor

159   genes were significantly elevated in LA-expressing rods (eg. *Rho*, *Gnat1*; Fig. 4E), and

160   significantly decreased in Lbr-expressing cells (eg. *Guca1a*, *Pde6b*; Fig. 4F). Nonetheless, the

161   overall magnitude of transcriptional changes in tethered rods was generally modest, with only a

162   few genes changing more than 2-fold. Interestingly, *Hist1h1c* and *Cbx3*, which encode key

163   heterochromatic proteins, were significantly downregulated in Lbr-expressing rods (Fig. 4F).

164

165   *Heterochromatin tethering regulates genome accessibility*

166

167 Previous studies have reported that rod photoreceptors uniquely exhibit megabase-scale

168 genomic intervals with unusually reduced chromatin accessibility[11]. We reasoned that this

169 unique accessibility signature might be altered by heterochromatin tethering. We therefore

170 performed ATAC-seq on rods transfected with control, LA, or Lbr constructs. To mark rods

171 specifically, we co-transfected the plasmids with a pRho2.2::DsRed reporter[28] (Fig. 4A, B). After

172 8 weeks, rod photoreceptors were sorted using EGFP, DsRed, and Dapi to mark viability.

173

174 Next, we processed the ATAC-seq datasets in order to call peaks. We first compared our

175 datasets against previously published ATAC-seq data from sorted rods[11]. In general, we

176 observed that all of our datasets exhibited comparable signal at the rod-specific peak loci

177 previously identified by Hughes et al.[11](Fig. S3). We also observed a lack of signal at the

178 promoters of several marker genes for non-rod cell types, such as cones, bipolars, and Müller

179 glia (Fig. S4).

180

181 In accordance with the hypothesis that inverted nuclear architecture restricts accessibility[11], we

182 observed an increase in the number of peaks in tethered rods (Fig. 4C). We compared LA or Lbr

183 -tethered rod ATAC-seq data versus normal rod datasets using two approaches. First, we

184 examined the overlap between peaks. We found that more than half of the rod-specific peaks

185 identified by Hughes et al. were shared by our ATAC-seq datasets (Fig. 4C). The control datasets

186 together contained less than 2000 peaks that were absent from tethered rods. By contrast, LA

187   and Lbr datasets exhibited 5094 and 6452 unique peaks, respectively, and shared an additional

188   7652 peaks – all of which were absent from the control datasets (Fig. 4C).

189

190   Secondly, we also plotted the data centered on the 35 858 LA peaks. This analysis revealed a

191   great deal of resemblance between the accessibility signatures of LA+ and Lbr+ rods. We

192   performed K-means clustering which allowed us to separate almost 10 000 peaks that had

193   markedly elevated signal in LA/Lbr tethered rods in comparison to controls (Fig. 4D; cluster C2;

194   arrows). Peak-to-gene annotation revealed that only ~10% of these novel peaks were found in

195   gene-proximal regions (Fig. S5A). Taken together, these analyses indicate that rods with

196   tethered heterochromatin gain thousands of additional peaks – mainly in distal intergenic

197   regions.

198

199   We inspected newly accessible peaks, but they did not appear to overlap with any specific

200   genomic feature. We therefore opted to perform footprinting analysis using the TOBIAS

201   algorithm[29]. TOBIAS examines ATAC-seq peaks to identify regions occluded by proteins, and to

202   match these 'footprints' to transcription factor motifs. We selected 220 transcription factor

203   motifs from the TRANSFAC database. Using this approach, we found that Ctcf footprints were

204   the most overrepresented motifs in both LA and Lbr datasets (Fig. S5B, C). Interestingly, rod-

205   specific transcription factor motifs such as Crx and Otx2 were overrepresented in the Lbr

206   dataset, but not LA-expressing rods. Focusing on novel tethering-specific cluster C2 peaks, we

207   next visualized Ctcf ChIP-seq datasets made from murine embryonic stem cells by the Bing Ren

208   lab[30]. We found that cluster C2 loci correlated with considerable Ctcf signal. These data suggest

209   that many of the peaks induced by heterochromatin tethering are genuine regulatory elements

210   that are normally decommissioned in rods.

211

212   Hughes et al. had also previously hypothesized that heterochromatin tethering might explain

213   the increased genomic accessibility of cones[11]. However, we found that in terms of genome

214   accessibility, tethered rods are more similar to control rods than to cones – perhaps not

215   surprisingly (Fig. S6A). Inspection of cone-specific peaks revealed that most remained

216   inaccessible in tethered rods (Fig. S6B; see also S4), except at the *Lmna* locus itself (Fig. S6C),

217   which was previously noted to be accessible in cones but not rods[11]. Some loci might therefore

218   take on cone-like accessibility signatures in response to tethering.

219

220   Finally, to address the hypothesis that heterochromatin tethering might affect the accessibility

221   of B compartment topologically associating domains (TADs), we examined rod-specific Hi-C

222   experiments[15]. Surprisingly, we found that almost all of the novel cluster C2 peaks were present

223   in the euchromatic A compartment (Fig. S7A). We did observe a few notable exceptions, where

224   B compartment accessibility was altered, including at the *Myc* gene (Fig. S7B), which was

225   previously reported to be localized within a large inaccessible interval[11], as well as across a TAD

226   that contains the chemokines *Ccl1*, *Ccl2*, *Ccl7*, *Ccl8*, *Ccl11*, and *Ccl12* (Fig. S7C). Nonetheless,

227   effects on B compartment accessibility were the exception.

228

229   *Heterochromatin tethering promotes accessibility at a subset of stress-responsive genes*

230

231   To understand how heterochromatin tethering might relate to function, we performed GO

232   terms analysis on the tethering-specific cluster C2 peaks using Panther and ReViGO[31, 32]. Since

233   almost 10 000 peaks were obtained in the cluster, peak-to-gene annotation would retrieve a

234   large proportion of genes in the genome. To reduce false discovery, we restricted our analysis

235   to gene-proximal peaks located from 5 kb upstream to 1 kb downstream of a given gene. This

236   reduced the overall peak count to only ~1400 peaks, corresponding to 500 genes. Significantly

237   enriched GO terms related to the stress response, including "immune response", "response to

238   wounding", and "inflammatory response" (Fig. 5A; Table S2).

239

240   To determine whether the same group of stress-responsive genes might upregulate in *rd1* rods,

241   we intersected the 500 tethering-specific cluster C2 genes with the RNA-seq data generated by

242   Jiang et al[21]. Only 25 genes within cluster C2 were significantly upregulated in *rd1* rods (Fig. 6B).

243   Moreover, we found little evidence for stress-responsive transcript upregulation in our Multi-

244   seq dataset (Fig. 6C, D). Nonetheless, a few cluster C2 genes exhibited notable increases in

245   accessibility, including the immediate early gene *Nab2* and the putative tumor suppressor *Tusc1*

246   (Fig. 6E, F; arrows). We also observed novel tethering-specific peaks at the *Ccl3* and *Ccl4*

247   chemokine genes (Fig. S8A) as well as the interferon activated gene *Ifi204* and the *Cd68* surface

248   marker (Fig. S8B, C), which were shown to become acutely accessible in a light damage model

249   of retinal degeneration[33]. Taken together, these data suggest that heterochromatin tethering

250   might 'poise' regulatory elements to facilitate the stress response, but that additional steps are

251   necessary for full gene activation.

252

Discussion

253   **Discussion**

254

255   The rod photoreceptors of nocturnal animals are perhaps the only eukaryotic cells that

256   normally function without heterochromatin tethering. However, disrupted nuclear organization

257   had been reported in a variety of mouse mutants for chromatin proteins[10, 12, 14, 15, 16, 17, 18]. A

258   similar reversal of nuclear organization occurs in *Nr2e3* and *Nrl* mutants, in which rods

259   transdifferentiate into cone-like photoreceptors[34, 35]. Here, we report that LA upregulates in the

260   *rd1* model of retinitis pigmentosa. Since *Pde6b* does not directly affect chromatin, we conclude

261   that *Lmna* upregulation can be a general response to degeneration.

262

263   How does LA upregulation affect the photoreceptor genome? Previous studies suggested that

264   the absence of tethering leads to a strikingly 'closed' accessibility signature[11, 36]. Perhaps

265   counterintuitively, our data suggest that tethering the heterochromatic B-compartment at the

266   nuclear periphery mainly affects accessibility within the euchromatic A-compartment. Acting

267   like the fingers in a "cat's cradle", heterochromatin tethering might be important for

268   disentangling and segregating B compartment TADs away from the A compartment (Fig. 7).

269   Alternatively, tethering might provide tensile force to chromosomes that could facilitate gene

270   expression. *LMNA* mutations have accordingly been shown to have extensive effects on

271   genome accessibility in other contexts[37].

272

273   Based on genome modelling, The Solovei and Mirny labs predicted that the introduction of

274   heterochromatin tethering in fully inverted rods would fail to restore conventional

14

275 architecture[15]. Results from *SCA7* and *Casz1* mutant mice, in which LA/LC upregulates in mature

276 rods agree with this prediction[12, 15]. By contrast, the upregulation of LA in *rd1* rods occurs prior

277 to full inversion. Nonetheless, since tethering mainly induced novel peaks within the A-

278 compartment, we predict that LA upregulation might have similar effects during the

279 degeneration of mature rods with fully inverted architecture.

280

281 *Heterochromatin tethers are permissive – but not instructive - for gene expression*

282

283 We found that LA/Lbr both increased genome accessibility similarly - mainly at distal intergenic

284 regions. Focusing on cluster C2 peaks, we found that Ctcf footprints were increased, suggesting

285 that these loci might be bona fide regulatory elements that are normally decommissioned in

286 inverted rods. Accordingly, we found that many these loci exhibited Ctcf occupancy in murine

287 ES cells. While the accessibility signatures of LA/Lbr were similar, they differed in footprint

288 enrichment profiles and differential gene expression. Moreover, morphometric analysis of

289 heterochromatin tethering revealed that Lbr had stronger effects on chromocenters. These

290 data might reflect differences in tethering mechanisms, and agree with previous research

291 indicating that LA/Lbr can have differential effects on gene expression[10].

292

293 One alternative possibility is that the increased accessibility observed in tethered rod datasets

294 might arise if samples were contaminated with non-rod cells. However, we disfavor this

295 interpretation. First, in our ATAC-seq experiments, we found that cell-type-specific marker

296 genes lacked accessibility, or exhibited equivalent accessibility when compared to control rod

297   datasets. Second, most of the observed novel peaks were distal to genes. Third, even for gene-

298   proximal peaks, GO terms were mainly associated with stress rather than cell fate, suggesting

299   that changes in cell composition are unlikely to account for the novel peaks.

300

301   Another alternative interpretation is that the observed accessibility signature might be a by-

302   product of toxicity introduced by construct overexpression. Again, we disfavor this scenario.

303   First, while LA/LC overexpression has been associated with toxicity, these effects are often

304   linked to mitotic catastrophe or nuclear rupture, which are mitigated in non-motile post-mitotic

305   rods. We harvested rods at least 6 weeks after transfection. The expression constructs were

306   thus tolerated in these cells over the long term. Second, similar changes in accessibility were

307   observed when rods were transfected with Lbr, which has been shown to be well-tolerated in

308   transgenic mice[9, 10]. Third, we examined transfections for cell death, but did not observe

309   pyknotic nuclei, elevated Dapi incorporation, or upregulation of stress-responsive gene

310   expression.

311

312   *Lamin A reorganizes the nucleus during degeneration*

313

314   ATAC-seq has been recently used to characterize degenerating retinas in age-related macular

315   degeneration and murine light damage models, revealing a marked *decrease* in genome

316   accessibility[33, 38]. Examination of RNA-seq data from the light damage model revealed that

317   *Lmna* was similarly upregulated by ~10-20 fold – both at 6 hours and one day post-injury, but

318   not at 3 days[33]. While the reported decrease in genomic accessibility thus conflicts with our

319   observations, the ATAC-seq data from the above studies were generated using whole retinas,

320   whereas we studied sorted rods. Moreover, we note that several genes that were reported to

321   become accessible upon light damage, including *Ccl4, Ifi204, and Cd68*, similarly became

322   accessible upon heterochromatin tethering via LA/Lbr (Fig. S8). Luu et al. also reported that

323   light damage increased accessibility at distal intergenic regions, in accordance with our

324   observations

325

326   Elsewhere in the CNS, changes in nuclear lamins have previously been linked to

327   neurodegeneration. For example, alterations in the expression and integrity of B-type lamins

328   have been documented in tauopathies and Alzheimer's disease[39, 40]. A potential linkage

329   between LA and photoreceptor degeneration nonetheless seemed unlikely, given that the

330   expression of the *LA* splice variant is usually suppressed in neurons[41], and has been repeatedly

331   shown to be absent in rods[10, 11, 12, 13]. However, LA was recently found to upregulate in

332   hippocampal neurons in Alzheimer's disease[42]. Indeed, *Lmna* upregulation was recently linked

333   to tissue damage in a variety of other organs[43], although the responsible regulatory

334   mechanisms have not yet been defined.

335

336   What might be the purpose of upregulating LA in response to pathology? Tethering

337   heterochromatin via LA/Lbr transfection appears to 'poise' the regulatory elements of stress-

338   responsive genes. However, the limited effect on transcription suggests that LA upregulation

339   may serve additional purposes. One possibility is that heterochromatin tethering may be

340   important for facilitating DNA repair. Indeed, previous studies have shown that DNA repair is

341   inefficient in inverted rod photoreceptors, and this inefficiency is ameliorated via transgenic

342   misexpression of Lbr[44, 45]. Given the well-documented linkage between LA/LC and DNA repair[46],

343   it would be interesting to test whether LA upregulation improves the efficiency of DNA repair

344   even further.

345

346 **Methods**

347

348 *Animals*

349

350 Animal work was conducted according to the guidelines of the Canadian Council on Animal Care

351 and the Animal Care and Veterinary Service at uOttawa using ethical protocols OHRI-2856 and

352 OHRI-2867. CD1 mice were obtained from Charles River Laboratories (Senneville QC, Canada).

353 *C57BL/6J* and *rd1* (C57BL/6J-*Pde6b*[rd1-2J]/J; strain# 004766) mice were obtained from Jackson

354 Laboratories (Bar Harbor ME) and maintained as homozygous stocks.

355

356 *DNA constructs*

357

358 pCIG2 and pCIG2 Lamin A were previously described[12, 47]. A pCIG2 Lbr plasmid was generated by

359 PCR amplifying Lbr from pMSCV-Flag-Lbr, generously provided by Peter Gaines[48] in order to

360 remove the Flag tag. Primers were Lbr XhoI F: 5'-CACACTCGAGATGCCAAGTAGGAAGTTTGTTG-3'

361 and Lbr EcoRI R: 5'- CACAGAATTCTCAGTAAATGTAGGGGAATATG-3'. To mark rod

362 photoreceptors, we utilized pRho-DsRed generously provided by Connie Cepko (Addgene

363 #11156)[28]. Stable cell lines were generated using pBABE-puro-GFP-wt-lamin A (Addgene

364 #17662) and pBABE-puro-GFP-Progerin (Addgene #17663) plasmids, generously shared by the

365 Tom Misteli lab[49].

366

367 *Electroporation*

368

369   In vivo retinal electroporations were performed as described previously[12, 28]. Briefly, P0 pups

370   were anesthetized on ice, and an incision was made into the eyelid to expose the orbit of the

371   eye. Plasmid DNA (2 μg/μl) was mixed with Fast Green dye and injected subretinally, using a

372   Femtojet microinjector (Eppendorf, Mississauga ON, Canada) and pulled borosilicate needles

373   (Drummond Scientific, Broomall, PA). Pups were placed into an incubator to re-warm, and then

374   replaced into the home cage.

375

376   *Flow cytometry*

377

378   Adult retinas were dissected and placed in StemPro Accutase (Thermo Fisher Scientific, Ottawa

379   ON, Canada) for 30 minutes at 37 °C. Cells were triturated manually, incubated with Dapi as a

380   viability marker, and then sorted by the OHRI Flow Cytometry and Cell Sorting Facility using a

381   MoFlo XDP (Beckman Coulter, Mississauga ON, Canada).

382

383   *Immunohistochemistry and microscopy*

384

385   Retinas were processed for immunohistochemistry as previously described[12, 50]. We used the

386   following primary antibodies: Nr2e3 (PNR: R&D Systems PP-H7223-00), lamin A (Fortis A303-

387   433A), and Lamin A/C (Harald Herrmann Lab). Hoechst 33342 (Tocris NB5117) and Alexa Fluor-

388   568-conjugated peanut agglutin (Molecular Probes L32458) were applied along with the

389   primary antibodies.

390

391   Images were acquired using Zeiss LSM880 or LSM900 confocal microscopes with Airyscan

392   detectors. All images presented in the paper are from individual Z-planes, and all level

393   transformations were linear. Images were processed using Zen (Zeiss), Fiji (ImageJ), and Adobe

394   Photoshop (Adobe) software. 3D reconstruction and animation was performed using IMARIS

395   v9.7 (Bitplane, South Windsor CT).

396

397   *Cell culture and western Blot*

398

399   Cell culture and western blotting were performed as previously described[12, 50]. See above for

400   antibody information. Stable cell lines expressing pBABE-puro-GFP-wt-lamin A**,** pBABE-puro-

401   GFP-Progerin, or a vector control plasmids were generated by transfecting 293 cells with

402   plasmids and selecting with puromycin (Bio Basic, Markham ON, Canada).

403

404   *Nuclear morphometric analysis*

405

406   Densitometry measurements were performed using ImageJ and Fiji software[51]. Single Airyscan

407   Z planes were analyzed. The perimeter of each selected nucleus was manually traced using the

408   "Freehand Selection" tool to first acquire the mean pixel intensity of the entire nuclear area.

409   Then, perimeters were re-traced using the "Freehand Line" tool, and the mean pixel intensity at

410   the nuclear perimeter was measured. This latter perimeter measurement was divided by the

411   mean pixel intensity of the entire nucleus in order to normalize each nucleus against variation

21

412   in image intensity. For the chromocenter midpoint/lamina measure, the distance between the

413   centroid of each chromocenter and the nuclear periphery was measured using the "Straight

414   Line" tool.

415

416   *Statistics*

417

418   Statistical analyses for count and measurement data were performed using Microsoft Excel and

419   GraphPad Prism 8 software. n-values refer to biological replicates (independent experiments,

420   animals, or cells as indicated in the text and figure legends). All error bars are mean ± SEM.

421

422   *ATAC-seq*

423

424   ATAC-seq data were generated following Buenrostro et al.[52]. Briefly, 50 000 flow-sorted cells

425   were lysed in cold lysis buffer (10 mM Tris-Cl, pH 7.4, 10 mM NaCl, 3 mM MgCl2 and 0.1%

426   IGEPAL CA-630). Lysed nuclei were tagmented using 6.5 µl of TDE1 transposase from the

427   Nextera DNA Flex Library kit (Illumina, Fredericton NB, Canada). Samples were purified using

428   Zymo-Spin IC columns (Zymo Research, Irvine CA), and libraries constructed according to the

429   Nextera workflow. Libraries were cleaned up using the AMPure XP kit (Beckman Coulter). PE

430   150 sequencing was performed using the NextSeq 500 platform to a read-depth of 25-35

431   million reads per sample.

432

433   *Multi-seq*

434

435 After flow cytometric sorting, cells were barcoded with 'anchor' and 'co-anchor' lipid-modified

436 oligonucleotides generously provided by the Zev Gartner lab[53]. Barcode oligonucleotides were

437 purchased from Integrated DNA Technologies (Coralville IA) as follows. Barcode 1: F: 5'-

438 CCTTGGCACCCGAGAATTCCAGGAGAAGAAAAAAAAAAAAAAAAAAAAAAAAAAAAAAAA-3'; Barcode

439 2: F: 5'- CCTTGGCACCCGAGAATTCCACCACAATGAGAAAAAAAAAAAAAAAAAAAAAAAAAAAAAAAA-

440 3'; Barcode 3: F: 5'-

441 CCTTGGCACCCGAGAATTCCATGAGACCTAAAAAAAAAAAAAAAAAAAAAAAAAAAAAAAA-3';

442

443 Each replicate was incubated with barcode oligonucleotides for 10 minutes. Cells were pelleted

444 and washed 3 times with PBS. Replicates were pooled and processed in a single 10X Genomics

445 (Pleasanton CA) Chromium run. Gene expression libraries were sequenced to an average depth

446 of 369 327 reads per cell. Expression library FASTQs were processed using CellRanger (10X

447 Genomics).

448

449 *Bioinformatics – ATAC-seq*

450

451 ATAC-seq Fastq files were processed via Fastq Groomer[54] and Trimmomatic[55], and then

452 mapped to the mm10 genome using Bowtie2[56]. Summit and narrowpeak calling was performed

453 with Macs2[57], and we used GREAT[58] for peak-to-gene annotation. GO terms analysis was

454 performed using Panther[31, 59] followed by ReViGO[32]. ATAC-seq histograms were generated

455 using Seqplots[60].

456

Sorted rod and double-sorted green cone ATAC-seq data and narrowpeak files (mm10) were

obtained from Hughes et al.[11] (GSE83312). Ctcf ChIP-seq data (ENCSR343RKY) generated by the

Bing Ren lab[30] were obtained from the ENCODE Consortium[61, 62].

460

For comparison with compartment data generated by Falk et al.[15] and Ctcf ChIP-seq data from

ENCODE, ATAC-seq data were re-mapped to the mm9 genome as per above, except that we

used Cutadapt for adapter trimming.

464

Footprinting analysis was performed using TOBIAS. As per the guidelines, we merged peak files

together: lamin A with control; Lbr with control. Bindetect was performed using 220 motifs

selected from the TRANSFAC database.

468

Bioinformatics – RNA-seq

470

RNA-seq data from sorted rod photoreceptors from P10 *Rd1* mice were obtained from Jiang et

al.[21] (GSE183117). Figure 1 presents the bioinformatic data published in the original paper. To

visualize *Lmna* transcription and splicing, we re-mapped the data to the mm9 genome using

Galaxy[63]. Fastq files were processed via Fastq Groomer[54] and Trimmomatic[55], and then mapped

to the mm9 genome using RNA Star[64]. Genome visualization and sashimi plots were generated

using IGV[65]. Heatmaps were generated using Morpheus

477 (https://software.broadinstitute.org/Morpheus). We quantitated differential transcripts using

478 FeatureCounts[66] and DeSeq2[67].

479

480 *Bioinformatics – scRNA-seq*

481

482 Fastq files were aligned to the mm10 genome using CellRanger version 6.1.2 (Cell Ranger

483 software, 10x Genomics). Output files were filtered and analyzed using Scanpy version 1.9.1[68] in

484 Python (Python Core Team n.d.). Genes detected in less than 3 cells were removed from the

485 analysis. Low-quality cells (less than 200 genes detected, more than 2500 genes detected or

486 more than 18% of mitochondrial genes) were also excluded. Scrublet version 0.2.2 was used to

487 detect doublets[69]. Replicates were demultiplexed with using the MULTI-seq workflow[53]. To

488 annotate cell types, we trained a deep learning model grounded on previously published retinal

489 single cell expression data[27] using scDeepSort version 1.0[26]. Mitochondrial gene regression and

490 initial gene expression analysis was performed using scVI-tools version 0.19.0[70]. Differential

491 gene expression analyses were performed using MAST version 1.24.0[71]. Data integration was

492 carried out on PostgreSQL version 14.3 (PostgreSQL Core Team n.d.) and Python's library

493 Pandas version 1.5.2 (Pandas Core Team n.d.).

494

495 **Author Contributions**

496

497 Conceptualization: I.N., A.F., P.M. Data curation: I.N., K.S., P.M. Formal analysis: all authors.

498 Investigation: I.N., K.S., P.M. Project administration, resources, supervision: P.M. Visualization:

499 A.F., I.N., P.M. Writing—original draft: P.M. Writing, review, and editing: all authors.

500

501 **Conflict of Interest:**

502

503 The authors declare no competing interests.

504

505 **Availability of Data and Materials:**

506

507 No restrictions on sharing data, reagents, or code. scRNA-seq and ATAC-seq datasets will be

508 uploaded to GEO.

509

510 **Acknowledgements**

511

526

Figure Legends

528

529 **Figure 1. Lamin A upregulates at the onset of rod degeneration in *rd1* rods.** (A, B)

530 Immunohistochemistry on wild-type C57BL/6 at P16 (A) or adult (B) stages using a LA-specific

531 antibody (white). The retina was counterstained for the rod marker Nr2e3 (A; green) or the

532 cone marker peanut agglutinin (B; green), as well as the DNA dye Hoechst 33342 (blue). Boxed

533 regions indicate the areas shown in the insets. Arrowheads indicate cone photoreceptors. (C, D)

534 Immunohistochemistry for LA or LA/LC (white) and the rod-specific marker Nr2e3 (green) on

535 *rd1* retinas at P16 (C) or P21 (D). Boxed regions indicate the areas shown in the insets. Arrows

536 indicate LA expression in Nr2e3+ rods. Scale bars = 10 μm. (E-H) Transcript expression at

537 different postnatal stages as indicated - from the Anand Swaroop lab (AS)[21]. (F) Sashimi plot of

538 splice junctions from P10 *rd1* RNA-seq data. (G, H) Transcription at the *Lmna* (G) or *Lbr* (H) loci

539 from P10 RNA-seq samples as indicated. Data were remapped from Jiang et al.[21] and plotted on

540 the same scale (group autoscale).

541

542 **Figure 2. Increased heterochromatin tethering in Lamin A+ *rd1* rods.** (A) Airyscan confocal

543 imaging of P16 *rd1* retinas stained for LA (white), Nr2e3 (green), and Hoechst (blue). Boxed

544 regions indicate the areas shown in (B, C). Arrowheads indicate LA+ Nr2e3+ rods. Arrows

545 indicate LA-negative Nr2e3+ rods. Asterisk indicates a pyknotic nucleus. Scale bars = 10 μm. (D)

546 Linear distance between chromocenter centroids and the nuclear margin. Nr2e3+ n=69

547 chromocenters from 30 cells; Nr2e3+ LA+ n=90 chromocenters from 30 cells; *** $p < 0.001$,

548 Mann-Whitney U test. (E) Mean chromatin intensity at the nuclear margin normalized against

549 the mean chromatin intensity of the nucleus. n=30 cells per group; **** p < 0.0001, Student's t-

550 test.

551

552 **Figure 3. Heterochromatin tethering by lamin A versus Lbr.** (A) In vivo electroporation

553 paradigm. Retinas were subretinally injected with plasmids, electroporated, and harvested after

554 6 weeks, yielding transfected rod photoreceptors. (B) Wholemount epifluorescence image of

555 EGFP expression from a transfected retina. (C) Morphometric analysis of transfected nuclei was

556 performed as indicated. (D) Densitometry values for chromatin intensity at the nuclear

557 periphery of Control (n=6) or LA -transfected cells (n=6) as indicated, obtained using the "Plot

558 profile" tool in Fiji. Each color represents a different cell. (E-G) Airyscan confocal imaging of rod

559 photoreceptors transfected with empty vector control (E), LA (F), or Lbr (G) expression

560 constructs, and harvested after 6 weeks. (H) Quantitation of chromatin intensity at the nuclear

561 margin measured using the "Freehand Line" tool in Fiji. Datapoints are the mean intensity

562 values from 3 independent transfections (30 cells each). **** p < 0.0001, ANOVA with Tukey's

563 post-hoc test. (I) Distance from the chromocenter midpoint to the nuclear periphery. n=56

564 untransfected; n=57 pCIG2; n=93 lamin A; n=77 Lbr. **** p < 0.0001, Kruskal-Wallace with

565 Dunn's post-hoc test.

566

567 **Figure 4. Comparison of gene expression in control versus tethered rods.** (A) UMAP projection

568 of Multi-seq dataset. (B) Unsupervised cell-type annotation via scDeepSort trained on a

569 previously published retinal scRNA-seq dataset[72]. (C) Demultiplexing of control, lamin A, and Lbr

570 samples. (D, E) Overlap of Control, lamin A, or Lbr -transfected cells within the rod cluster. (F, G)

571   Volcano plots of differential gene expression in annotated rods. (F) Lamin A versus control. (G)

572   Lbr versus control.

573

574   **Figure 5. Heterochromatin tethering promotes chromatin accessibility.** (A) In vivo

575   electroporation paradigm. Retinas were subretinally injected with expression plasmids,

576   including the rod-specific pRho2.2-DsRed reporter. Electroporated retinas were harvested after

577   8 weeks, yielding DsRed+ rod photoreceptors. (B) Wholemount epifluorescence image of EGFP

578   and DsRed expression from a transfected retina. (C) Upset plot of of ATAC-seq peak

579   intersections from sorted rods transfected with control, LA, or Lbr expression constructs

580   compared against previously published data from the Joe Corbo lab (JC)[11] as indicated. (D)

581   Alignment of ATAC-seq data from sorted rods transfected with control, LA, or Lbr expression

582   constructs compared against previously published data as indicated. Plots are centered on peak

583   summits from LA transfected rods. Arrows indicate the tethering-specific cluster C2 peaks.

584

585   **Figure 6. Heterochromatin tethering promotes accessibility at stress responsive genes.** (A) GO

586   terms analysis of tethering-specific cluster C2 genes (see Fig. 4D) via PantherDB and ReViGO.

587   Peak-to-gene annotation was restricted to gene proximal peaks as described in the text. (B)

588   Intersection of RNA-seq data from control versus *rd1* sorted rods intersected with annotated

589   (gene-proximal) cluster C2 genes. Heatmap values are transformed by subtracting the row

590   median and dividing by the median absolute deviation. (C, D) Expression changes for selected

591   stress-responsive genes, comparing RNA-seq data from control versus *rd1* sorted rods from the

592   Anand Swaroop lab (AS)[21] (C) versus scRNA-seq data from rods transfected with control, lamin

593   A, or Lbr plasmids (D). (E, F) Control vs. *rd1* RNA-seq, and ATAC-seq tracks and called peaks

594   from Hughes et al. (JC)[11], compared against ATAC-seq tracks generated from control, LA, or Lbr -

595   transfected rods at the *Nab2* (E) and *Tusc1* (F) loci. RNA-seq and ATAC-seq tracks were

596   respectively group-autoscaled. Arrows indicate peaks present specifically in tethered rods, but

597   not control rods.

598

599   **Figure 7. Cat's cradle model for tethering-dependent effects on genome accessibility.** (A)

600   During the differentiation of wild-type rods, the tethering of heterochromatin (dark blue) by Lbr

601   (purple) stretches the chromosomes, promoting accessibility in the A-compartment (cyan).

602   Over time, Lbr expression is downregulated leading to chromatin relaxation, and finally

603   chromatin inversion. As the chromatin relaxes, accessibility decreases. (B) During the

604   differentiation of *rd1* rods, lamin A (red) upregulates at the onset of tissue damage. The

605   prolongation of tethering promotes accessibility at genomic regions that would normally be

606   decommissioned. *Rd1* rods downregulate lamin A prior to cell death.

607

References

608

609   1.   Wong-Riley MT. Energy metabolism of the visual system. *Eye and brain* 2010, **2:** 99-116.

610

611   2.   Reingruber J, Holcman D, Fain GL. How rods respond to single photons: Key adaptations

612   of a G-protein cascade that enable vision at the physical limit of perception. *Bioessays*

613   2015, **37**(11)**:** 1243-1252.

614

615   3.   Hsiau TH, Diaconu C, Myers CA, Lee J, Cepko CL, Corbo JC. The cis-regulatory logic of the

616   mammalian photoreceptor transcriptional network. *PloS one* 2007, **2**(7)**:** e643.

617

618   4.   Siegert S, Cabuy E, Scherf BG, Kohler H, Panda S, Le YZ*, et al.* Transcriptional code and

619   disease map for adult retinal cell types. *Nature neuroscience* 2012, **15**(3)**:** 487-495, S481-

620   482.

621

622   5.   Eberhart A, Feodorova Y, Song C, Wanner G, Kiseleva E, Furukawa T*, et al.* Epigenetics of

623   eu- and heterochromatin in inverted and conventional nuclei from mouse retina.

624   *Chromosome research : an international journal on the molecular, supramolecular and*

625   *evolutionary aspects of chromosome biology* 2013, **21**(5)**:** 535-554.

626

627   6.   Kizilyaprak C, Spehner D, Devys D, Schultz P. In vivo chromatin organization of mouse

628   rod photoreceptors correlates with histone modifications. *PloS one* 2010, **5**(6)**:** e11039.

629

630   7.   Solovei I, Kreysing M, Lanctot C, Kosem S, Peichl L, Cremer T*, et al.* Nuclear architecture

631   of rod photoreceptor cells adapts to vision in mammalian evolution. *Cell* 2009, **137**(2)**:**

632   356-368.

633

634   8.   Smith CL, Lan Y, Jain R, Epstein JA, Poleshko A. Global chromatin relabeling accompanies

635   spatial inversion of chromatin in rod photoreceptors. *Sci Adv* 2021, **7**(39)**:** eabj3035.

636

637   9.   Subramanian K, Weigert M, Borsch O, Petzold H, Garcia-Ulloa A, Myers EW*, et al.* Rod

638   nuclear architecture determines contrast transmission of the retina and behavioral

639   sensitivity in mice. *eLife* 2019, **8**.

640

641   10.   Solovei I, Wang AS, Thanisch K, Schmidt CS, Krebs S, Zwerger M*, et al.* LBR and lamin A/C

642   sequentially tether peripheral heterochromatin and inversely regulate differentiation.

643   *Cell* 2013, **152**(3)**:** 584-598.

644

645   11.   Hughes AE, Enright JM, Myers CA, Shen SQ, Corbo JC. Cell Type-Specific Epigenomic

646   Analysis Reveals a Uniquely Closed Chromatin Architecture in Mouse Rod

647   Photoreceptors. *Scientific reports* 2017, **7:** 43184.

648

649   12.   Mattar P, Stevanovic M, Nad I, Cayouette M. Casz1 controls higher-order nuclear

650   organization in rod photoreceptors. *Proceedings of the National Academy of Sciences of*

651   *the United States of America* 2018, **115**(34)**:** E7987-E7996.

652

653   13.   Razafsky DS, Ward CL, Kolb T, Hodzic D. Developmental regulation of linkers of the

654   nucleoskeleton to the cytoskeleton during mouse postnatal retinogenesis. *Nucleus*

655   2013, **4**(5)**:** 399-409.

656

657   14.   Barabino A, Plamondon V, Abdouh M, Chatoo W, Flamier A, Hanna R*, et al.* Loss of Bmi1

658   causes anomalies in retinal development and degeneration of cone photoreceptors.

659   *Development* 2016, **143**(9)**:** 1571-1584.

660

661   15.   Falk M, Feodorova Y, Naumova N, Imakaev M, Lajoie BR, Leonhardt H*, et al.*

662   Heterochromatin drives compartmentalization of inverted and conventional nuclei.

663   *Nature* 2019, **570**(7761)**:** 395-399.

664

665   16.   Helmlinger D, Hardy S, Abou-Sleymane G, Eberlin A, Bowman AB, Gansmuller A*, et al.*

666   Glutamine-expanded ataxin-7 alters TFTC/STAGA recruitment and chromatin structure

667   leading to photoreceptor dysfunction. *PLoS biology* 2006, **4**(3)**:** e67.

668

669   17.   Popova EY, Grigoryev SA, Fan Y, Skoultchi AI, Zhang SS, Barnstable CJ. Developmentally

670   regulated linker histone H1c promotes heterochromatin condensation and mediates

671   structural integrity of rod photoreceptors in mouse retina. *The Journal of biological*

672   *chemistry* 2013, **288**(24)**:** 17895-17907.

673

674 18. Tran NM, Zhang A, Zhang X, Huecker JB, Hennig AK, Chen S. Mechanistically distinct

675   mouse models for CRX-associated retinopathy. *PLoS genetics* 2014, **10**(2)**:** e1004111.

676

677 19. Swamy VS, Fufa TD, Hufnagel RB, McGaughey DM. Building the mega single-cell

678   transcriptome ocular meta-atlas. *Gigascience* 2021, **10**(10).

679

680 20. McLaughlin ME, Sandberg MA, Berson EL, Dryja TP. Recessive mutations in the gene

681   encoding the beta-subunit of rod phosphodiesterase in patients with retinitis

682   pigmentosa. *Nature genetics* 1993, **4**(2)**:** 130-134.

683

684 21. Jiang K, Mondal AK, Adlakha YK, Gumerson J, Aponte A, Gieser L*, et al.* Multiomics

685   analyses reveal early metabolic imbalance and mitochondrial stress in neonatal

686   photoreceptors leading to cell death in Pde6brd1/rd1 mouse model of retinal

687   degeneration. *Human molecular genetics* 2022, **31**(13)**:** 2137-2154.

688

689 22. Farinelli P, Perera A, Arango-Gonzalez B, Trifunovic D, Wagner M, Carell T*, et al.* DNA

690   methylation and differential gene regulation in photoreceptor cell death. *Cell death &*

691   *disease* 2014, **5:** e1558.

692

693 23. de Melo J, Peng GH, Chen S, Blackshaw S. The Spalt family transcription factor Sall3

694   regulates the development of cone photoreceptors and retinal horizontal interneurons.

695   *Development* 2011, **138**(11)**:** 2325-2336.

696

24. Emerson MM, Surzenko N, Goetz JJ, Trimarchi J, Cepko CL. Otx2 and Onecut1 promote the fates of cone photoreceptors and horizontal cells and repress rod photoreceptors. *Developmental cell* 2013, **26**(1)**:** 59-72.

700

25. Javed A, Mattar P, Lu S, Kruczek K, Kloc M, Gonzalez-Cordero A*, et al.* Pou2f1 and Pou2f2 cooperate to control the timing of cone photoreceptor production in the developing mouse retina. *Development* 2020, **147**(18).

704

26. Shao X, Yang H, Zhuang X, Liao J, Yang P, Cheng J*, et al.* scDeepSort: a pre-trained cell-type annotation method for single-cell transcriptomics using deep learning with a weighted graph neural network. *Nucleic acids research* 2021, **49**(21)**:** e122.

708

27. Clark BS, Stein-O'Brien GL, Shiau F, Cannon GH, Davis-Marcisak E, Sherman T*, et al.* Single-Cell RNA-Seq Analysis of Retinal Development Identifies NFI Factors as Regulating Mitotic Exit and Late-Born Cell Specification. *Neuron* 2019, **102**(6)**:** 1111-1126 e1115.

712

28. Matsuda T, Cepko CL. Electroporation and RNA interference in the rodent retina in vivo and in vitro. *Proceedings of the National Academy of Sciences of the United States of America* 2004, **101**(1)**:** 16-22.

716

717   29.   Bentsen M, Goymann P, Schultheis H, Klee K, Petrova A, Wiegandt R*, et al.* ATAC-seq

718   footprinting unravels kinetics of transcription factor binding during zygotic genome

719   activation. *Nature communications* 2020, **11**(1)**:** 4267.

720

721   30.   He Y, Hariharan M, Gorkin DU, Dickel DE, Luo C, Castanon RG*, et al.* Spatiotemporal DNA

722   methylome dynamics of the developing mouse fetus. *Nature* 2020, **583**(7818)**:** 752-759.

723

724   31.   Gene Ontology C. The Gene Ontology resource: enriching a GOld mine. *Nucleic acids*

725   *research* 2021, **49**(D1)**:** D325-D334.

726

727   32.   Supek F, Bosnjak M, Skunca N, Smuc T. REVIGO summarizes and visualizes long lists of

728   gene ontology terms. *PloS one* 2011, **6**(7)**:** e21800.

729

730   33.   Luu J, Kallestad L, Hoang T, Lewandowski D, Dong Z, Blackshaw S*, et al.* Epigenetic

731   hallmarks of age-related macular degeneration are recapitulated in a photosensitive

732   mouse model. *Human molecular genetics* 2020, **29**(15)**:** 2611-2624.

733

734   34.   Corbo JC, Cepko CL. A hybrid photoreceptor expressing both rod and cone genes in a

735   mouse model of enhanced S-cone syndrome. *PLoS genetics* 2005, **1**(2)**:** e11.

736

737   35.   Mears AJ, Kondo M, Swain PK, Takada Y, Bush RA, Saunders TL*, et al.* Nrl is required for

738   rod photoreceptor development. *Nature genetics* 2001, **29**(4)**:** 447-452.

739

740   36.   Aldiri I, Xu B, Wang L, Chen X, Hiler D, Griffiths L*, et al.* The Dynamic Epigenetic

741   Landscape of the Retina During Development, Reprogramming, and Tumorigenesis.

742   *Neuron* 2017, **94**(3)**:** 550-568 e510.

743

744   37.   Kohler F, Bormann F, Raddatz G, Gutekunst J, Corless S, Musch T*, et al.* Epigenetic

745   deregulation of lamina-associated domains in Hutchinson-Gilford progeria syndrome.

746   *Genome medicine* 2020, **12**(1)**:** 46.

747

748   38.   Wang J, Zibetti C, Shang P, Sripathi SR, Zhang P, Cano M*, et al.* ATAC-Seq analysis reveals

749   a widespread decrease of chromatin accessibility in age-related macular degeneration.

750   *Nature communications* 2018, **9**(1)**:** 1364.

751

752   39.   Frost B, Bardai FH, Feany MB. Lamin Dysfunction Mediates Neurodegeneration in

753   Tauopathies. *Current biology : CB* 2016, **26**(1)**:** 129-136.

754

755   40.   Matias I, Diniz LP, Damico IV, Araujo APB, Neves LDS, Vargas G*, et al.* Loss of lamin-B1

756   and defective nuclear morphology are hallmarks of astrocyte senescence in vitro and in

757   the aging human hippocampus. *Aging cell* 2022, **21**(1)**:** e13521.

758

759   41.   Jung HJ, Coffinier C, Choe Y, Beigneux AP, Davies BS, Yang SH*, et al.* Regulation of

760   prelamin A but not lamin C by miR-9, a brain-specific microRNA. *Proceedings of the*

761   *National Academy of Sciences of the United States of America* 2012, **109**(7)**:** E423-431.

762

763   42.   Gil L, Nino SA, Chi-Ahumada E, Rodriguez-Leyva I, Guerrero C, Rebolledo AB*, et al.*

764   Perinuclear Lamin A and Nucleoplasmic Lamin B2 Characterize Two Types of

765   Hippocampal Neurons through Alzheimer's Disease Progression. *Int J Mol Sci* 2020,

766   **21**(5).

767

768   43.   Machado L, Geara P, Camps J, Dos Santos M, Teixeira-Clerc F, Van Herck J*, et al.* Tissue

769   damage induces a conserved stress response that initiates quiescent muscle stem cell

770   activation. *Cell stem cell* 2021, **28**(6)**:** 1125-1135 e1127.

771

772   44.   Frohns A, Frohns F, Naumann SC, Layer PG, Lobrich M. Inefficient double-strand break

773   repair in murine rod photoreceptors with inverted heterochromatin organization.

774   *Current biology : CB* 2014, **24**(10)**:** 1080-1090.

775

776   45.   Frohns F, Frohns A, Kramer J, Meurer K, Rohrer-Bley C, Solovei I*, et al.* Differences in the

777   Response to DNA Double-Strand Breaks between Rod Photoreceptors of Rodents, Pigs,

778   and Humans. *Cells* 2020, **9**(4).

779

780   46.   Gonzalo S. DNA damage and lamins. *Advances in experimental medicine and biology*

781   2014, **773:** 377-399.

782

783   47.   Hand R, Bortone D, Mattar P, Nguyen L, Heng JI, Guerrier S*, et al.* Phosphorylation of

784   Neurogenin2 specifies the migration properties and the dendritic morphology of

785   pyramidal neurons in the neocortex. *Neuron* 2005, **48**(1)**:** 45-62.

786

787   48.   Subramanian G, Chaudhury P, Malu K, Fowler S, Manmode R, Gotur D*, et al.* Lamin B

788   receptor regulates the growth and maturation of myeloid progenitors via its sterol

789   reductase domain: implications for cholesterol biosynthesis in regulating myelopoiesis.

790   *Journal of immunology* 2012, **188**(1)**:** 85-102.

791

792   49.   Scaffidi P, Misteli T. Lamin A-dependent misregulation of adult stem cells associated

793   with accelerated ageing. *Nature cell biology* 2008, **10**(4)**:** 452-459.

794

795   50.   Mattar P, Jolicoeur C, Dang T, Shah S, Clark BS, Cayouette M. A Casz1-NuRD complex

796   regulates temporal identity transitions in neural progenitors. *Scientific reports* 2021,

797   **11**(1)**:** 3858.

798

799   51.   Schneider CA, Rasband WS, Eliceiri KW. NIH Image to ImageJ: 25 years of image analysis.

800   *Nature methods* 2012, **9**(7)**:** 671-675.

801

802   52.   Buenrostro JD, Wu B, Chang HY, Greenleaf WJ. ATAC-seq: A Method for Assaying

803   Chromatin Accessibility Genome-Wide. *Curr Protoc Mol Biol* 2015, **109:** 21 29 21-21 29

804   29.

805

806   53.   McGinnis CS, Patterson DM, Winkler J, Conrad DN, Hein MY, Srivastava V*, et al.* MULTI-

807   seq: sample multiplexing for single-cell RNA sequencing using lipid-tagged indices.

808   *Nature methods* 2019, **16**(7)**:** 619-626.

809

810   54.   Blankenberg D, Gordon A, Von Kuster G, Coraor N, Taylor J, Nekrutenko A*, et al.*

811   Manipulation of FASTQ data with Galaxy. *Bioinformatics* 2010, **26**(14)**:** 1783-1785.

812

813   55.   Bolger AM, Lohse M, Usadel B. Trimmomatic: a flexible trimmer for Illumina sequence

814   data. *Bioinformatics* 2014, **30**(15)**:** 2114-2120.

815

816   56.   Langmead B, Salzberg SL. Fast gapped-read alignment with Bowtie 2. *Nature methods*

817   2012, **9**(4)**:** 357-359.

818

819   57.   Feng J, Liu T, Qin B, Zhang Y, Liu XS. Identifying ChIP-seq enrichment using MACS. *Nature*

820   *protocols* 2012, **7**(9)**:** 1728-1740.

821

822   58.   McLean CY, Bristor D, Hiller M, Clarke SL, Schaar BT, Lowe CB*, et al.* GREAT improves

823   functional interpretation of cis-regulatory regions. *Nature biotechnology* 2010, **28**(5)**:**

824   495-501.

825

826   59.   Ashburner M, Ball CA, Blake JA, Botstein D, Butler H, Cherry JM*, et al.* Gene ontology:

827   tool for the unification of biology. The Gene Ontology Consortium. *Nature genetics*

828   2000, **25**(1)**:** 25-29.

829

830   60.   Stempor P, Ahringer J. SeqPlots - Interactive software for exploratory data analyses,

831   pattern discovery and visualization in genomics. *Wellcome Open Res* 2016, **1:** 14.

832

833   61.   Consortium EP. An integrated encyclopedia of DNA elements in the human genome.

834   *Nature* 2012, **489**(7414)**:** 57-74.

835

836   62.   Luo Y, Hitz BC, Gabdank I, Hilton JA, Kagda MS, Lam B*, et al.* New developments on the

837   Encyclopedia of DNA Elements (ENCODE) data portal. *Nucleic acids research* 2020,

838   **48**(D1)**:** D882-D889.

839

840   63.   Afgan E, Baker D, van den Beek M, Blankenberg D, Bouvier D, Cech M*, et al.* The Galaxy

841   platform for accessible, reproducible and collaborative biomedical analyses: 2016

842   update. *Nucleic acids research* 2016, **44**(W1)**:** W3-W10.

843

844   64.   Dobin A, Davis CA, Schlesinger F, Drenkow J, Zaleski C, Jha S*, et al.* STAR: ultrafast

845   universal RNA-seq aligner. *Bioinformatics* 2013, **29**(1)**:** 15-21.

846

847   65.   Thorvaldsdottir H, Robinson JT, Mesirov JP. Integrative Genomics Viewer (IGV): high-

848   performance genomics data visualization and exploration. *Briefings in bioinformatics*

849   2013, **14**(2)**:** 178-192.

850

851   66.   Liao Y, Smyth GK, Shi W. featureCounts: an efficient general purpose program for

852   assigning sequence reads to genomic features. *Bioinformatics* 2014, **30**(7)**:** 923-930.

853

854   67.   Love MI, Huber W, Anders S. Moderated estimation of fold change and dispersion for

855   RNA-seq data with DESeq2. *Genome biology* 2014, **15**(12)**:** 550.

856

857   68.   Wolf FA, Angerer P, Theis FJ. SCANPY: large-scale single-cell gene expression data

858   analysis. *Genome biology* 2018, **19**(1)**:** 15.

859

860   69.   Wolock SL, Lopez R, Klein AM. Scrublet: Computational Identification of Cell Doublets in

861   Single-Cell Transcriptomic Data. *Cell Syst* 2019, **8**(4)**:** 281-291 e289.

862

863   70.   Gayoso A, Lopez R, Xing G, Boyeau P, Valiollah Pour Amiri V, Hong J*, et al.* A Python

864   library for probabilistic analysis of single-cell omics data. *Nature biotechnology* 2022,

865   **40**(2)**:** 163-166.

866

867 71.   Finak G, McDavid A, Yajima M, Deng J, Gersuk V, Shalek AK*, et al.* MAST: a flexible

868   statistical framework for assessing transcriptional changes and characterizing

869   heterogeneity in single-cell RNA sequencing data. *Genome biology* 2015, **16:** 278.
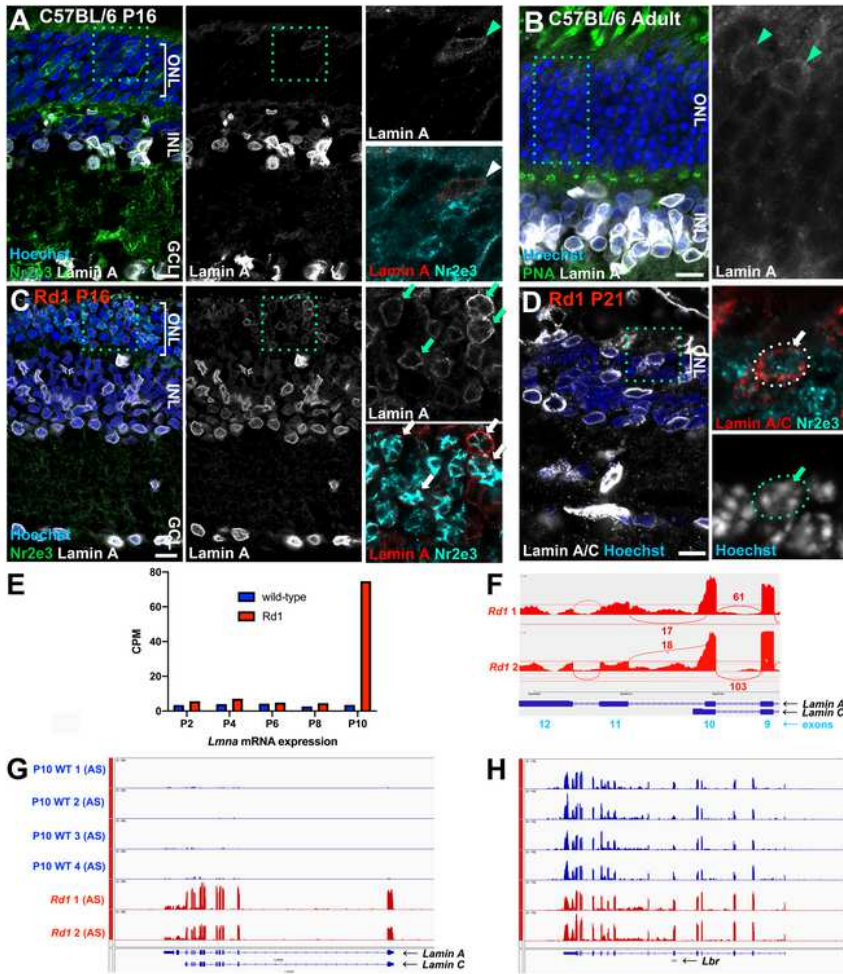
870

871 72.   Clark BS, Stein-O'Brien GL, Shiau F, Cannon GH, Davis-Marcisak E, Sherman T*, et al.*

872   Single-Cell RNA-Seq Analysis of Retinal Development Identifies NFI Factors as Regulating

873   Mitotic Exit and Late-Born Cell Specification. *Neuron* 2019.

874

875

Figures

Nađ et al. Fig. 1

Figure 1. Lamin A upregulates at the onset of rod degeneration in *rd1* rods. (A, B)
Immunohistochemistry on wild-type C57BL/6 at P16 (A) or adult (B) stages using a LA-specific
antibody (white). The retina was counterstained for the rod marker Nr2e3 (A; green) or the
cone marker peanut agglutinin (B; green), as well as the DNA dye Hoechst 33342 (blue). Boxed
regions indicate the areas shown in the insets. Arrowheads indicate cone photoreceptors. (C, D)
Immunohistochemistry for LA or LA/LC (white) and the rod-specific marker Nr2e3 (green) on
rd1 retinas at P16 (C) or P21 (D). Boxed regions indicate the areas shown in the insets. Arrows
indicate LA expression in Nr2e3+ rods. Scale bars = 10 μm. (E-H) Transcript expression at
different postnatal stages as indicated - from the Anand Swaroop lab (AS)[21]. (F) Sashimi plot of
splice junctions from P10 *rd1* RNA-seq data. (G, H) Transcription at the *Lmna* (G) or *Lbr* (H) loci
from P10 RNA-seq samples as indicated. Data were remapped from Jiang et al.[21] and plotted on
the same scale (group autoscale).
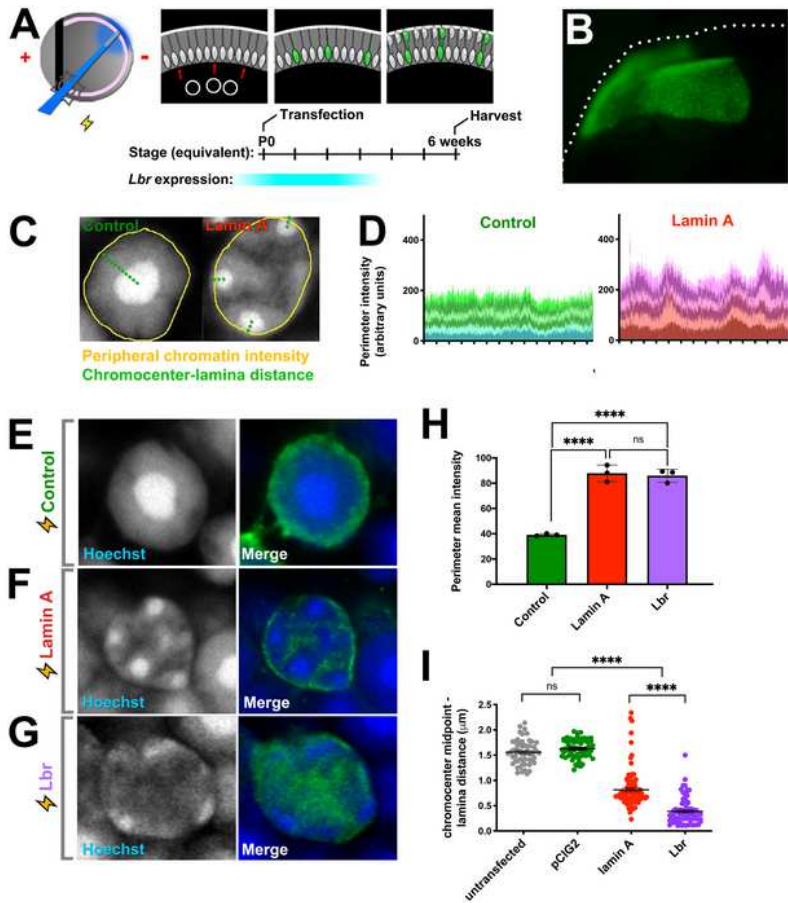
Figure 1

See image above for figure legend
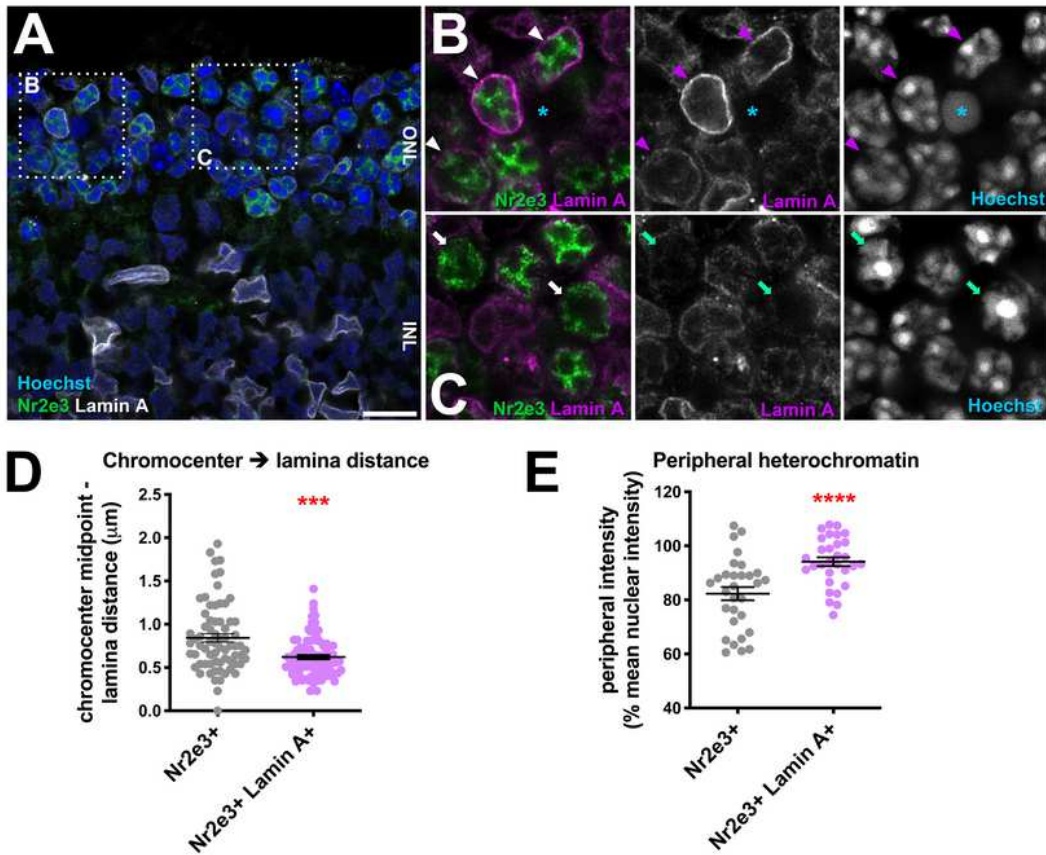
Naď et al. Fig. 2

Figure 2. Increased heterochromatin tethering in Lamin A+ *rd1* rods. (A) Airyscan confocal imaging of P16 *rd1* retinas stained for LA (white), Nr2e3 (green), and Hoechst (blue). Boxed regions indicate the areas shown in (B, C). Arrowheads indicate LA+ Nr2e3+ rods. Arrows indicate LA-negative Nr2e3+ rods. Asterisk indicates a pyknotic nucleus. Scale bars = 10 μm. (D) Linear distance between chromocenter centroids and the nuclear margin. Nr2e3+ n=69 chromocenters from 30 cells; Nr2e3+ LA+ n=90 chromocenters from 30 cells; *** p < 0.001, Mann-Whitney U test. (E) Mean chromatin intensity at the nuclear margin normalized against the mean chromatin intensity of the nucleus. n=30 cells per group; **** p < 0.0001, Student's t-test.

Figure 2

See image above for figure legend

Naď et al. Fig. 3

Figure 3. Heterochromatin tethering by lamin A versus Lbr. (A) In vivo electroporation paradigm. Retinas were subretinally injected with plasmids, electroporated, and harvested after 6 weeks, yielding transfected rod photoreceptors. (B) Wholemount epifluorescence image of EGFP expression from a transfected retina. (C) Morphometric analysis of transfected nuclei was performed as indicated. (D) Densitometry values for chromatin intensity at the nuclear periphery of Control (n=6) or LA -transfected cells (n=6) as indicated, obtained using the "Plot profile" tool in Fiji. Each color represents a different cell. (E-G) Airyscan confocal imaging of rod photoreceptors transfected with empty vector control (E), LA (F), or Lbr (G) expression constructs, and harvested after 6 weeks. (H) Quantitation of chromatin intensity at the nuclear margin measured using the "Freehand Line" tool in Fiji. Datapoints are the mean intensity values from 3 independent transfections (30 cells each). **** p < 0.0001, ANOVA with Tukey's post-hoc test. (I) Distance from the chromocenter midpoint to the nuclear periphery. n=56 untransfected; n=57 pCIG2; n=93 lamin A; n=77 Lbr. **** p < 0.0001, Kruskal-Wallace with Dunn's post-hoc test.

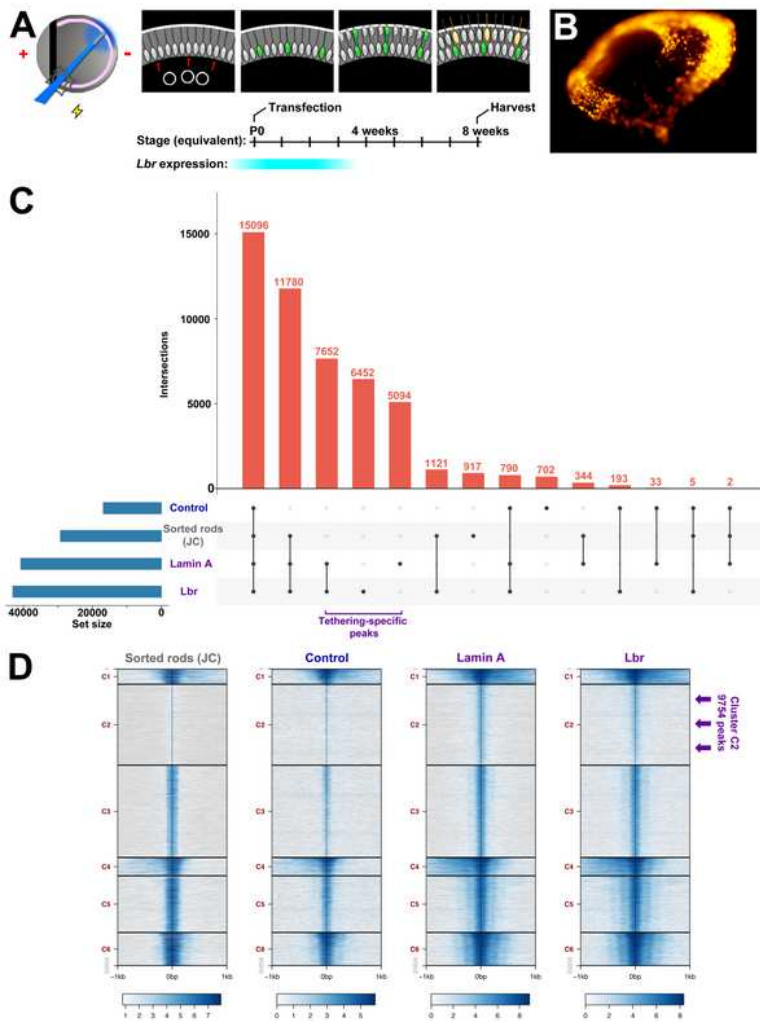# Figure 3

See image above for figure legend
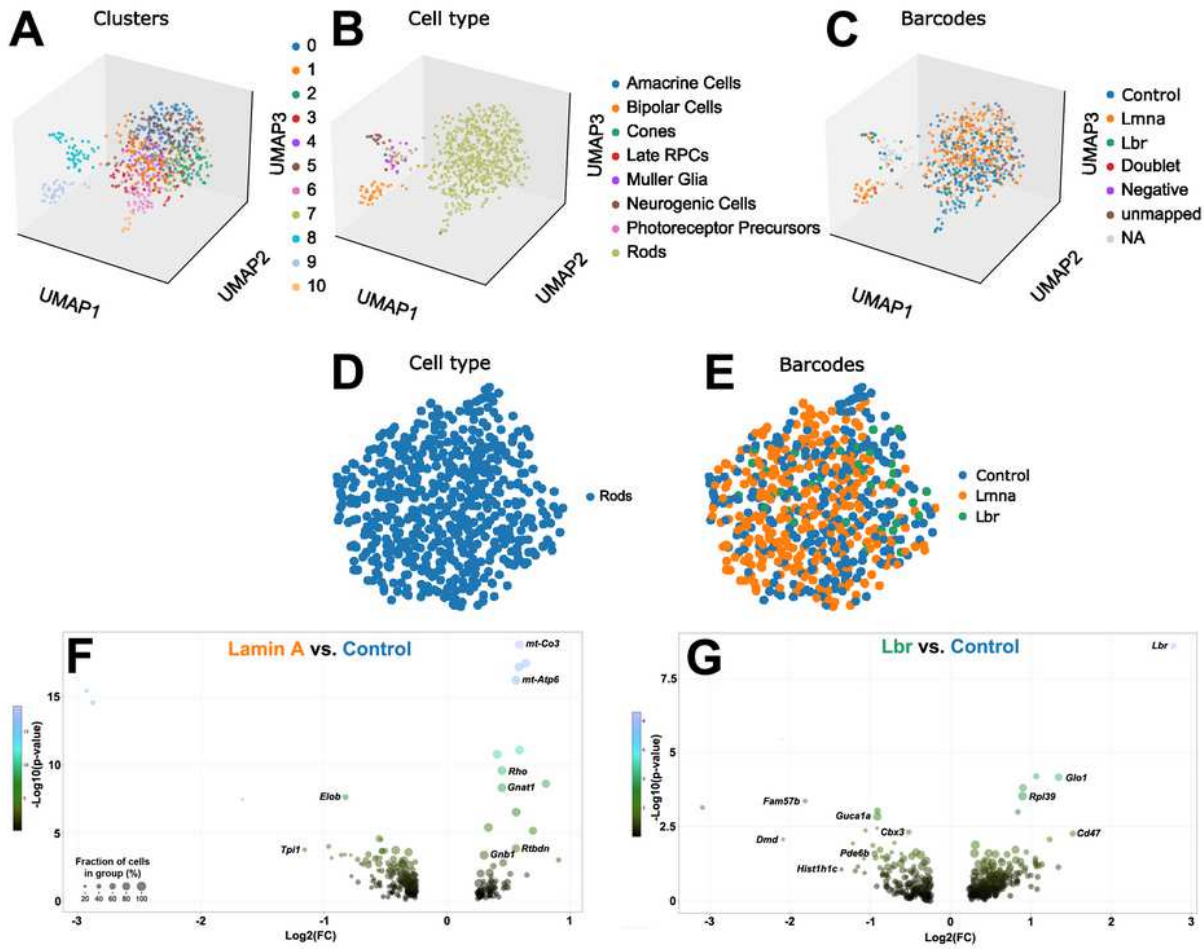
Figure 4. Comparison of gene expression in control versus tethered rods. (A) UMAP projection of Multi-seq dataset. (B) Unsupervised cell-type annotation via scDeepSort trained on a previously published retinal scRNA-seq dataset[72]. (C) Demultiplexing of control, lamin A, and Lbr samples. (D, E) Overlap of Control, lamin A, or Lbr -transfected cells within the rod cluster. (F, G) Volcano plots of differential gene expression in annotated rods. (F) Lamin A versus control. (G) Lbr versus control.
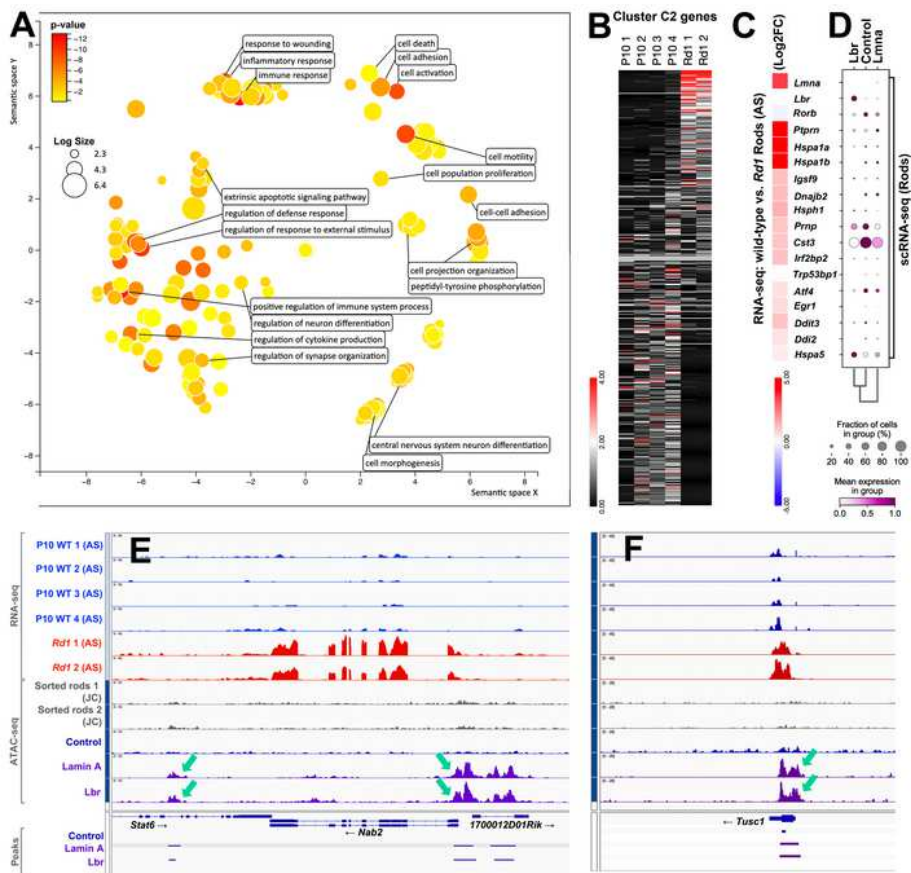
Figure 4

See image above for figure legend

Nađ et al. Fig. 5

Figure 5. Heterochromatin tethering promotes chromatin accessibility. (A) In vivo electroporation paradigm. Retinas were subretinally injected with expression plasmids, including the rod-specific pRho2.2-DsRed reporter. Electroporated retinas were harvested after 8 weeks, yielding DsRed+ rod photoreceptors. (B) Wholemount epifluorescence image of EGFP and DsRed expression from a transfected retina. (C) Upset plot of of ATAC-seq peak intersections from sorted rods transfected with control, LA, or Lbr expression constructs compared against previously published data from the Joe Corbo lab (JC)[11] as indicated. (D) Alignment of ATAC-seq data from sorted rods transfected with control, LA, or Lbr expression constructs compared against previously published data as indicated. Plots are centered on peak summits from LA transfected rods. Arrows indicate the tethering-specific cluster C2 peaks.
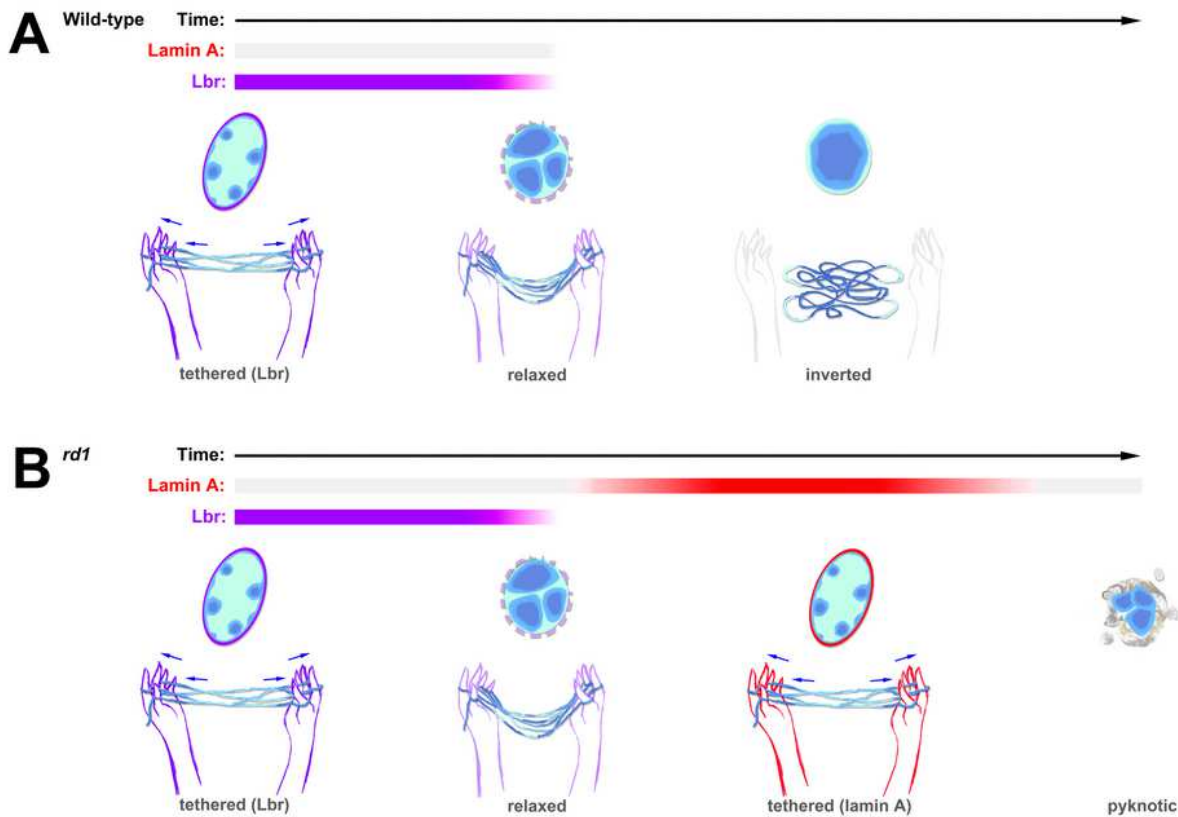
Figure 5

See image above for figure legend

Nađ et al. Fig. 6

Figure 6. Heterochromatin tethering promotes accessibility at stress responsive genes. (A) GO terms analysis of tethering-specific cluster C2 genes (see Fig. 4D) via PantherDB and ReViGO. Peak-to-gene annotation was restricted to gene proximal peaks as described in the text. (B) Intersection of RNA-seq data from control versus *rd1* sorted rods intersected with annotated (gene-proximal) cluster C2 genes. Heatmap values are transformed by subtracting the row median and dividing by the median absolute deviation. (C, D) Expression changes for selected stress-responsive genes, comparing RNA-seq data from control versus *rd1* sorted rods from the Anand Swaroop lab (AS)[21] (C) versus scRNA-seq data from rods transfected with control, lamin A, or Lbr plasmids (D). (E, F) Control vs. *rd1* RNA-seq, and ATAC-seq tracks and called peaks from Hughes et al. (JC)[11], compared against ATAC-seq tracks generated from control, LA, or Lbr - transfected rods at the *Nab2* (E) and *Tusc1* (F) loci. RNA-seq and ATAC-seq tracks were respectively group-autoscaled. Arrows indicate peaks present specifically in tethered rods, but not control rods.

Figure 6

See image above for figure legend

Figure 7. Cat's cradle model for tethering-dependent effects on genome accessibility. (A) During the differentiation of wild-type rods, the tethering of heterochromatin (dark blue) by Lbr (purple) stretches the chromosomes, promoting accessibility in the A-compartment (cyan). Over time, Lbr expression is downregulated leading to chromatin relaxation, and finally chromatin inversion. As the chromatin relaxes, accessibility decreases. (B) During the differentiation of *rd1* rods, lamin A (red) upregulates at the onset of tissue damage. The prolongation of tethering promotes accessibility at genomic regions that would normally be decommissioned. *Rd1* rods downregulate lamin A prior to cell death.

Figure 7

See image above for figure legend

Supplementary Files

This is a list of supplementary files associated with this preprint. Click to download.

- P16Rd1nr2e3gbethyllaminArairyscanstack1.avi
- SupplementalTable1.xlsx
- Supplementaltable2.xlsx
- Supplementalsection.pdf